**Ocean Systems Engineering**, *Vol. 16, No. 2 (2026) 139-168*
https://doi.org/10.12989/ose.2026.16.2.139

Techno-Press

# Analysis of installation of suction caissons in multilayered sand and silt using a classical bearing capacity method

Hiroyoshi Hirai*

*Applied Geotechnical Institute, Inc., 1808, Oizumi, Hokuto, Yamanashi, 409-1502, Japan*

*(Received July 29, 2024, Revised May 20, 2026, Accepted May 22, 2026)*

**Abstract.** There have been few analytical research studies to elucidate the effect of a low-permeability soil layer on the suction-induced seepage flow in the sand layer during the installation of suction caissons in multilayered soils. In this study, the influence of silt on penetration into the sand layer during suction caisson installation in multilayered sand and silt was investigated using a classical bearing capacity method. Since sand liquefaction tends to occur during suction installation, the relationship between suction and penetration was revealed in both preliquefaction and postliquefaction. The experimental results so far indicated that the unit shaft and base resistances of piles do not necessarily increase with depth, but instead reach maximum values at a certain critical depth. Thus, the friction reduction factors along the caisson skirt and the bearing capacity reduction factors at the caisson tip were presented for installation with both hardening and softening. Furthermore, an analytical procedure for punching shear failure in the silt layer overlying a sand layer during installation was proposed. For the relationships between suction and penetration during installation in multilayered sand and silt, a comparison between the results obtained from field and centrifuge tests and those predicted by the proposed method was carried out.

**Keywords:** bearing capacity; centrifuge tests; classical method; installation; sand and silt; suction caisson

## 1. Introduction

Suction caissons are widely used for foundations and anchors of offshore wind turbines. During self-weight installation, a caisson penetrates into the seabed via its own weight. During the installation of suction caissons in sand, suction-induced seepage plays a pivotal role, assisting the penetration by reducing soil resistance. In practice, the relative density and the stresses in the soil surrounding the caisson are affected by the installation. The installation effect is assumed to be insignificant compared with the caisson response under the general loadings. For suction caissons set on 'wished-in-place' in the post-installation, large numbers of research works have been carried out when the caissons are subjected to the vertical, horizontal, and moment loads, e.g., Hirai [1-8]. However, despite their wide use, some issues and uncertainties have been addressed for installation in layered soils where sands are overlain by low-permeability soils.

For a variety of irregular seabed topography and soil conditions encountered in shallow and deep seas, most design procedures regarding caisson installation often adopt the assumption of a homogeneous, isotropic seabed profile; e.g., Erbrich and Tjelta [9], Houlsby and Byrne [10, 11],

*Corresponding author, Ph.D., E-mail: ojiken@eps4.comlink.ne.jp


http://www.techno-press.org/ose/5

ISSN: 2093-6702 (Print), 2093-677X (Online)

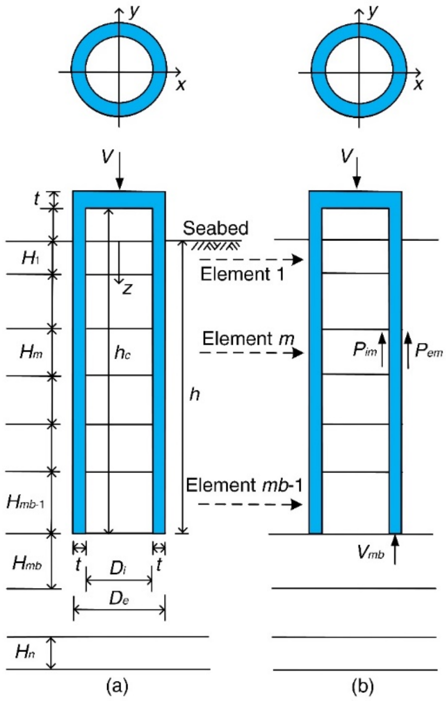


Figure 1. (a) Suction caisson and (b) discretization in nonhomogeneous soil under vertical compressive load during installation

Senders and Randolph [12], Koteras and Ibsen [13], and Rodriguez et al. [14]. However, to achieve feasible installation in a complex site that includes soils with a layered profile, it is critical to investigate the mechanism of how penetration resistance in high-permeability soil is affected by low-permeability soil.

The effect of a low-permeability soil layer on suction-induced seepage flow in a sand layer is not clearly understood. There have been very few research studies of caisson installation in layered soils. By conducting centrifuge tests with an acceleration of 100 g, Tran [15] and Tran et al. [16] investigated the suction trend during installation in sand layers with interbedded silt layers. Performing tests in a geotechnical centrifuge such that the stress levels are realistic and relevant to field conditions, Ragni et al. [17] and Stapelfeldt et al. [18] revealed the mechanism and characteristics of caisson installation in both clay overlain by sand and sand overlain by clay. However, there has been little analytical approach to predict the characteristics during the installation of suction caissons in multilayered sand and low-permeability soil.

In this study, for multilayered sand and silt, the effect of silt layer on suction caisson installation in sand is investigated analytically using a classical bearing capacity method premised on yield and failure theories. Because sand liquefaction tends to occur during suction installation, the relationships between suction and penetration are revealed for installation during both preliquefaction and postliquefaction. The experimental results performed by Kerisel [19], Vesić [20], the BCP Committee [21], Hanna and Tan [22], and Zhang et al. [23] indicated that the unit shaft and base resistances of piles do not necessarily increase with depth, but instead reach maximum values at a certain critical depth and do not increase beyond this depth. Therefore, the friction reduction factors along the caisson skirt and the bearing capacity reduction factors at the caisson tip are presented for installation with both hardening and softening. Since the vertical load applied to a shallow foundation on the sand layer overlying a clay layer sometimes causes punching shear failure [24], [25], which breaks through the sand layer into the clay layer, an analytical procedure of punching shear failure in the silt layer overlying a sand layer during installation is proposed. For the relationships between suction and penetration during installation in multilayered sand and silt, a comparison between the results obtained from field and centrifuge tests and those predicted by the present method was carried out.

Fig. 1(a) shows a cylindrical suction caisson in nonhomogeneous soil during installation. The geometry of the suction caisson is as follows: the external diameter is $D_e$, the internal diameter is $D_i$, each thickness of the lid and skirt is $t$, the skirt length is $h_c$, and the penetration depth from the seabed to the skirt tip is $h$. A vertical compressive load ($V$) is applied on the top center of the lid. The seabed is assumed to comprise the $n$ layers of nonhomogeneous soil with length $H_m$ in the $m$th layer. The $mb$-th soil layer is located under the tip of a caisson. The rectangular Cartesian coordinate system ($x, y, z$) on the reference point (0, 0, 0) is arranged such that the $z$-axis is in the direction of depth.

Fig. 1(b) shows discretization of a suction caisson and a nonhomogeneous soil subjected to vertical compressive load on the top of the lid during installation. The vertical force along the $m$th discretized element is denoted as $P_{Vm}$, which is composed of the internal traction, $P_{im}$, and the external traction, $P_{em}$, along the caisson wall, i.e., $P_{Vm} = P_{im} + P_{em}$. The tip of the caisson skirt experiences the vertical force $V_{mb}$ on the $mb$-th layer.

## 2. Vertical stress

The configuration of a suction caisson during installation is shown in Fig. 2. Fig. 3 shows the vertical equilibrium of an internal soil disc with area $A_i$ and depth $dz$ within the skirt.

The equilibrium equation was presented by Janssen [26] as follows

$$\frac{d\sigma'_{zi}}{dz} = \mu_i \sigma'_{zi} + \gamma'_i \tag{1}$$

where $\sigma'_{zi}$ is the effective vertical pressure inside the skirt and

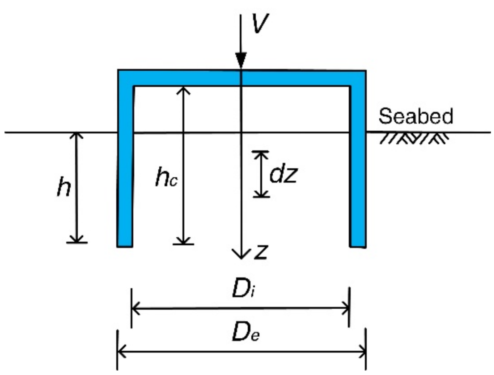


Figure 2. Configuration of suction caisson during installation

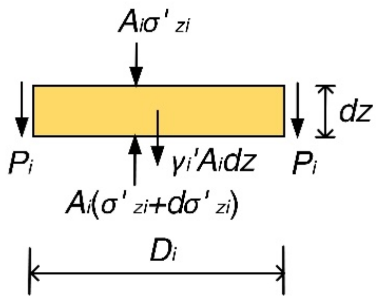


Figure 3. Vertical equilibrium of soil disc within skirt

$$\mu_i = \frac{4K_S tan\delta}{D_i} \tag{2}$$

where $K_S$ is the coefficient of lateral pressure and $\delta$ is the interface friction angle between the soil and skirt. Taking into account the effective unit weight of soil, $\gamma'$, and the excess pore pressure (suction), $s$, $\gamma_i'$ is defined as

$$\gamma_i' = \gamma' - \frac{(1-a)s}{h} \tag{3}$$

where $a$ is the pressure factor given by Houlsby and Byrne [11]. The solution of Eq. (1) can be described as

$$\sigma'_{zi} = \gamma_i'/\mu_i(e^{\mu_i z} - 1) \tag{4}$$

The effective vertical pressure outside the skirt $\sigma'_{ze}$ was presented by Houlsby and Byrne [11] as follows

$$\sigma'_{ze} = \gamma_e'/\mu_e(e^{\mu_e z} - 1) \tag{5}$$

where

$$\mu_e = \frac{4K_S tan\delta}{D_e(m^2-1)} \tag{6}$$

and $m$ is the modification factor, and $\gamma_e'$ is given by taking into account the effective unit weight of soil and suction as follows

$$\gamma_e' = \gamma' + \frac{as}{h} \tag{7}$$

## 3. Yield and base failure

The vertical yield resistance of soil outside skirt $P_{Vye}(z)$ and that of soil inside skirt $P_{Vyi}(z)$ per unit length along the skirt of the suction caisson under a vertical force can be written as follows

$$P_{Vye}(z) = \pi K_S \tan\delta\, \sigma'_{ze} D_e \tag{8}$$

$$P_{Vyi}(z) = \pi K_S \tan\delta\, \sigma'_{zi} D_i \tag{9}$$

The frictional forces outside and inside the skirt are obtained by the integral of the vertical yield resistances given by Eqs. (8) and (9), respectively, along the penetration depth. Since the silt used in the experiments conducted by Tran [15] and Tran et al. [16] was assumed to be nonplastic and noncohesive as well as sand, this assumption is adopted in the present research. For the base failure of sand and silt subjected to vertical stress, the ultimate base resistance (bearing capacity) $\sigma_{zu}$ outside the skirt, $\sigma_{zue}$, and that inside the skirt, $\sigma_{zui}$, are written as

$$\sigma_{zue} = 0.5\gamma_e' t N_\gamma + \sigma_{be}' N_q \tag{10}$$

$$\sigma_{zui} = 0.5\gamma_i' t N_\gamma + \sigma_{bi}' N_q \tag{11}$$

where $N_\gamma$ is the bearing capacity factor given by Michalowski [27] as follows

$$N_\gamma = exp(0.66 + 5.11\, tan\,\varphi)\, tan\,\varphi \tag{12}$$

where $N_q = K_p \exp(\pi\tan\varphi)$ is the bearing capacity factor presented by Reissner [28], $K_p$ is the coefficient of the Rankine passive pressure defined as $(1+\sin\varphi)/(1-\sin\varphi)$, $\varphi$ is the angle of the internal friction of soil, and $\sigma'_{be}$ and $\sigma'_{bi}$ are the effective vertical stresses in the soil outside and inside the skirt at the level of the caisson tip, respectively. By employing a classical bearing capacity theory that includes the four factors corresponding to the bearing capacity, shape, depth, and inclination, Hirai [5, 6, 8] proposed an analytical approach for suction caissons in sand subjected to vertical, lateral, and moment loads.

Using the buoyant weight of the suction caisson, $W_c$, the suctions under the lid and the skirt tip, the frictional forces inside and outside the skirt, and the bearing capacity on the annulus of the caisson tip, $Q_{tip}$, the equilibrium of these forces exerted on the suction caisson during installation can be written as

$$\begin{aligned} W_c + \frac{s\pi D_i^2}{4} + \frac{as\pi\left(D_e^2 - D_i^2\right)}{4} &= \frac{\pi D_i^2}{4}\sum_{j=1}^{m_b-1}\gamma_{ij}'\left\{\frac{e^{\mu_{ij}h_j} - e^{\mu_{ij}h_{j-1}}}{\mu_{ij}} - H_j\right\} + \\ &\frac{\pi D_e^2\left(m^2-1\right)}{4}\sum_{j=1}^{m_b-1}\gamma_{ej}'\left\{\frac{e^{\mu_{ej}h_j} - e^{\mu_{ej}h_{j-1}}}{\mu_{ej}} - H_j\right\} + Q_{tip} \end{aligned} \tag{13}$$

where $h_j$ is the depth of the $j$th layer's bottom, and $\gamma'_{ij}$, $\gamma'_{ej}$, $\mu_{ij}$, and $\mu_{ej}$ are $\gamma'_i$, $\gamma'_e$, $\mu_i$, and $\mu_e$ of the $j$th layer, respectively. The bearing capacity $Q_{tip}$ is given as follows

$$Q_{tip} = \sigma_{zu} t\pi(D_i + D_e)/2 \tag{14}$$

where $\sigma_{zu}$ denotes the smaller of the bearing capacities of Eqs. (10) and (11).

## 4. Liquefaction

If the applied suction in the caisson is $s$ with respect to the ambient seabed water pressure, then the absolute pressure in the caisson is represented as $p_a + \gamma_w h_w - s$, where $p_a$ is the atmospheric pressure, $\gamma_w$ is the unit weight of water, and $h_w$ is the water depth. Liquefaction tends to occur during suction installation following self-weight installation. Taking into account the equations presented by Houlsby and Byrne [11], the relationships between suction and penetration during both preliquefaction and postliquefaction can be determined using the equilibrium of forces given by Eq. (13). In particular, the suction is simply related to the penetration for postliquefaction as follows

$$s = \frac{\gamma' h}{1 - a} \tag{15}$$

where $a$, which is the pressure factor at the tip of the caisson, is given by

$$a = \frac{a_1 k_f}{1 + a_1 (k_f - 1)} \tag{16}$$

Here, $a_1$, which was proposed by Houlsby and Byrne [11], is the pressure factor; and $k_f = k_i / k_e$, which is the ratio of the permeability for the soil inside the caisson, $k_i$, to that for the soil outside the caisson, $k_e$.

Houlsby and Byrne [11] presented a calculation procedure to predict the installation of a suction caisson in sand. This procedure adopts the modification factor $m$ related to a zone between diameters $D_e$ and $D_m = mD_e$, where the vertical stress is enhanced due to the action of the downward friction from the caisson.

## 5. Vertical friction and bearing capacity

It is known that the unit shaft and base resistances of piles do not necessarily increase with depth, but instead reach maximum values at a certain critical depth and do not increase beyond this depth; e.g., Kerisel [19], Vesić [20], the BCP Committee [21], Hanna and Tan [22], and Zhang et al. [23]. By taking into account this behavior, an investigation into the value of $K_S \tan\delta$ in Eqs. (8) and (9) will be made, because the unit shaft resistance is obtained from the value of $K_S \tan\delta$ times the effective vertical stress. The installation of a suction caisson is achieved by producing a sequence of the ultimate states where the failure of soil below the skirt tip and the yield of soil along the skirt occur simultaneously. The movement of a caisson caused by suction installation is much larger and more complex compared to the displacement of the caisson generated by the infinitesimal and finite deformations due to external loads. This is the reason why the specific various assumptions regarding the value of $K_S \tan\delta$ during installation are needed to predict the complicated soil behavior during the installation process in layered soils, as will be mentioned below.

If the penetration of the caisson increases with increasing suction, installation with hardening (e.g., Pande and Zienkiewicz [29]) occurs. This behavior is attributed to the hardening of soil during plastic deformation. Experimental results by Tran [15] and Tran et al. [16] suggested that following the onset of sand liquefaction during installation of suction caissons in sand and silt layers, the value of $K_S \tan\delta$ during installation with hardening tends to decrease with increasing penetration. In this case, the depth of the onset of sand liquefaction is considered to correspond to the critical depth.

When the suction caisson penetrates into the silt layer overlying a sand layer, the suction often reaches a peak value at a certain penetration depth during installation with hardening, while the skirt tip is still in the silt layer. After arriving at the peak of suction, the penetration of the caisson increases with decreased suction until the tip reaches the sand layer below the silt layer. This is referred to as installation with softening (e.g., Pande and Zienkiewicz [29]). This behavior is ascribed to the softening of soil during plastic deformation. The installation of a suction caisson in layered soils is accompanied by a sequence of softening subsequent to hardening of surrounding soils. Therefore, it is postulated in the current study that there are three kinds of processes during

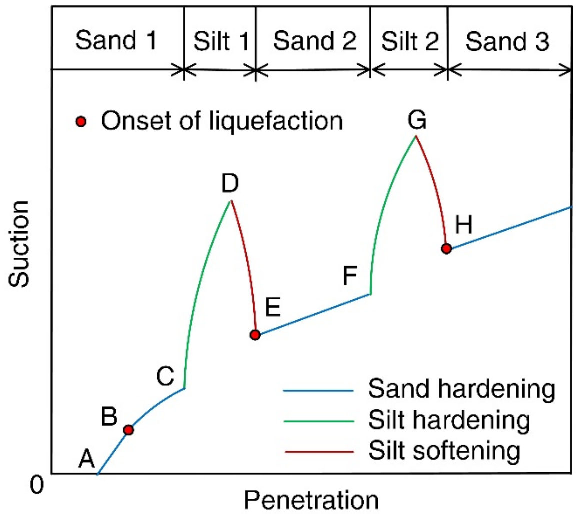


Figure 4. Relationships between penetration and suction schematically shown during installation of suction caissons through two silt layers in three sand layers

installation of suction caissons in multilayered sand and silt, i.e., (1) Sand hardening, (2) Silt hardening, and (3) Silt softening.

Fig. 4 illustrates the relationships between penetration and suction schematically shown during installation of suction caissons through two silt layers in three sand layers. The caisson settles at point $A$ during self-weight installation. The suction installation begins and the caisson tip arrives at point $B$ of the onset of liquefaction in sand 1. The installation process from point $A$ to $C$ causes hardening in sand 1. The installation from point $C$ to $D$ with a peak value of suction corresponds to hardening in silt 1. Softening in silt 1 occurs from point $D$ to $E$ being the surface of sand 2. The instant that the tip penetrates into sand 2, seepage flow and liquefaction occur because of the scouring of silt 1. The suction increases again with further penetration from point $E$ to $F$ during hardening in sand 2. Hardening from point $F$ to $G$ in silt 2, softening from point $G$ to $H$ in silt 2, and hardening from point $H$ in sand 3 occur during installation.

For multilayered sand and silt illustrated in Fig. 4, when the caisson tip penetrates into the depth of $h$ in the $k$-th soil layer, the value of $(K_S \tan\delta)_i$ in the $i$-th $(i \le k)$ soil layer the depth of which is shallower than or equal to that of the $k$-th soil layer may be represented in the following form

$$(K_S\, tan\delta)_i = Fh_k \cdot (K_S\, tan\delta)_{iN} \tag{17}$$

where $Fh_k$, which is the friction reduction factor at the caisson tip in the $k$-th soil layer, is equal to one before sand liquefaction and smaller than one following liquefaction, and $(K_S \tan\delta)_{iN}$ is the value for the $i$-th soil layer specified initially.

In the following, an investigation into the friction reduction factor, $Fh_k$, is made for the multilayered sand and silt shown in Fig. 4. To predict the characteristics during installation of suction caissons in multilayered sand and silt, it is postulated in the present study that (1) During the installation keeping the caisson tip in the silt layer, no seepage flow occurs because of the low permeability of the silt layer. (2) At the instant when the skirt tip penetrates through the silt layer into the lower sand layer, seepage flow and liquefaction occur due to the scouring of the silt layer.

### 5.1 The first sand hardening

For the first layer of sand, using Eq. (17), the value of $K_S\tan\delta$ at the caisson tip in the first layer of sand during installation with hardening, $(K_S\tan\delta)_{H1}$, may be assumed as follows

$$(K_S\, tan\delta)_{Hk} = Fh_k\, (K_S\, tan\delta)_{kN} \quad (k = 1) \tag{18}$$

$$Fh_k = Kh_{Hk} \quad (k = 1) \tag{19}$$

where $Kh_{H1}$ is the friction factor at the caisson tip in the first layer of sand during installation with hardening, as will be mentioned below.

The experimental results of suction caissons provided by Tran [15] and Tran et al. [16] suggested that the friction factor tends to reduce with increasing penetration and suction during installation with hardening in sand and silt layers following sand liquefaction. From taking into account this behavior, a simple form of the friction factor, $Kh_{H1}$, at the caisson tip following liquefaction in the first layer of sand may be inferred as follows

$$Kh_{Hk} = \frac{s_{kL}}{s_k}\{1 - \beta(1 - \frac{h_{kL}}{h_k})\} \quad (k = 1) \tag{20}$$

where $s_{1L}$ and $h_{1L}$ are the suction and the depth at the onset of liquefaction in the first layer of sand, respectively, $s_1$ and $h_1$ are the suction and the penetration at the caisson tip following liquefaction in the first layer of sand, respectively, and $\beta$ is a hardening constant.

The experimental data given by Tran [15] and Tran et al. [16] indicated that during installation of suction caissons in sand and silt layers, hardening develops until the caisson tip reaches the peak of suction in the silt layer, i.e., until punching shear failure occurs, as will be mentioned below. This leads to the inference that installation with hardening in sand and silt layers following sand liquefaction may induce a reduction in the bearing capacity on the caisson tip in sand and silt layers, as mentioned above for the base resistance of piles.

Thus, the bearing capacity on the caisson tip during installation with hardening in the first layer of sand, which is expressed as $\sigma_{zuH1}$, may be inferred in a simple form employing the friction reduction factor $Fh_1$ given by Eqs. (19) and (20) as follows

$$\sigma_{zuHk} = f_{BHk}\sigma_{zu} \quad (k = 1) \tag{21}$$

$$f_{BHk} = exp(Fh_k - 1) \quad (k = 1) \tag{22}$$

where $f_{BH1}$ is the bearing capacity reduction factor on the caisson tip in the first layer of sand.

### 5.2 The first silt hardening

Using Eq. (17), the value of $K_S\tan\delta$ at the caisson tip in the second layer of silt during installation with hardening subsequent to installation with hardening in the first layer of sand, which is written as $(K_S\tan\delta)_{H2}$, may be assumed in a simple form as follows

$$(K_S\, tan\delta)_{Hk} = Fh_k \cdot\, (K_S\, tan\delta)_{kN} \quad (k = 2) \tag{23}$$

$$Fh_k = Kh_{Hk} \quad (k = 2) \tag{24}$$

where the friction factor, $Kh_{H2}$, at the caisson tip in the second layer of silt during installation with hardening after liquefaction in the first layer of sand may be represented as follows

$$Kh_{Hk} = \frac{s_{(k-1)L}}{s_k}\{1 - \beta(1 - \frac{h_{(k-1)L}}{h_k})\} \quad (k = 2) \tag{25}$$

where $s_2$ and $h_2$ are the suction and the penetration at the caisson tip in the second layer of silt, respectively.

Accordingly, the bearing capacity on the caisson tip during installation with hardening in the second layer of silt, which is expressed as $\sigma_{zuH2}$, may be assumed utilizing the friction reduction factor $Fh_2$ given by Eq. (24) as follows

$$\sigma_{zuHk} = f_{BHk}\sigma_{zu} \quad (k = 2) \tag{26}$$

$$f_{BHk} = exp(Fh_k - 1) \quad (k = 2) \tag{27}$$

where $f_{BH2}$ is the bearing capacity reduction factor on the caisson tip in the second layer of silt.

The peak suction and the depth at the peak suction in the second layer of silt during installation with hardening are denoted by $s_{2P}$ and $h_{2P}$, respectively.

### 5.3 The first silt softening

The value of $K_S\tan\delta$ at the caisson tip during installation with softening in the second layer of silt subsequent to installation with hardening in the second layer of silt, which is represented as $(K_S\tan\delta)_{S2}$, may be assumed in a simple form as follows

$$(K_S\, tan\delta)_{Sk} = Fh_k \cdot (K_S\, tan\delta)_{kN} \quad (k = 2) \tag{28}$$

$$Fh_k = Kh_{Sk} \cdot Kh_{HkP} \quad (k = 2) \tag{29}$$

where $Kh_{S2}$, which is the friction factor at the caisson tip in the second layer of silt during installation with softening, will be presented below, and $Kh_{H2P}$ is given by Eq. (25) with $s_2 = s_{2P}$ and $h_2 = h_{2P}$.

The experimental results of suction caissons provided by Tran [15] and Tran et al. [16] suggested that $Kh_{S2}$ in Eq. (29) during installation with softening tends to decrease with increasing penetration and decreasing suction. From considering this behavior, a simple form of $Kh_{S2}$ may be inferred as follows

$$Kh_{Sk} = 1 - \zeta(1 - \frac{h_{kP}}{h_k}\frac{s_k}{s_{kP}}) \quad (k = 2) \tag{30}$$

where $\zeta$ is a softening constant.

The experimental data given by Tran [15] and Tran et al. [16] indicated that during installation with softening in the silt layer overlying a sand layer, sand liquefaction tends to occur inside skirts when the caisson tip reaches the sand layer below the silt layer. In this case, the bearing capacity on the caisson tip in the silt layer decreases and eventually reaches zero due to liquefaction of the underlying sand. Taking into account this behavior, the bearing capacity on the caisson tip in the second layer of silt during installation with softening, which is written as $\sigma_{zuS2}$, may be assumed utilizing the friction reduction factor $Fh_2$ given by Eq. (29) in a simple form as follows

$$\sigma_{zuSk} = f_{BSk}\sigma_{zu} \qquad (k = 2) \tag{31}$$

$$f_{BSk} = \frac{h_{kB} - h_k}{h_{kB} - h_{kP}} Fh_k \qquad (k = 2) \tag{32}$$

where $f_{BS2}$ is the bearing capacity reduction factor on the caisson tip in the second layer of silt and $h_{2B}$ is the depth from the seabed to the bottom of the second layer of silt. The suction at the bottom of the second layer of silt is denoted by $s_{2B}$.

### 5.4 The second sand hardening

The value of $K_S\tan\delta$ at the caisson tip in the third layer of sand during installation with hardening subsequent to installation with softening in the second layer of silt, which is written as $(K_S\tan\delta)_{H3}$, may be assumed in a simple form as follows:

$$(K_S\,tan\delta)_{Hk} = Fh_k \cdot (K_S\,tan\delta)_{kN} \qquad (k = 3) \tag{33}$$

$$Fh_k = Kh_{Hk} \cdot Kh_{S(k-1)B} \cdot Kh_{H(k-1)P} \qquad (k = 3) \tag{34}$$

where $Kh_{S2B}$ is given by Eq. (30) with $s_2 = s_{2B}$ and $h_2 = h_{2B}$, and similarly to Eq. (20) for the first sand hardening, $Kh_{H3}$ is represented by

$$Kh_{Hk} = \frac{s_{kL}}{s_k}\{1 - \beta(1 - \frac{h_{kL}}{h_k})\} \qquad (k = 3) \tag{35}$$

where $s_{3L}$ and $h_{3L}$ are the suction and the depth at the onset of liquefaction in the third layer of sand, respectively, and $s_3$ and $h_3$ are the suction and the penetration at the caisson tip following liquefaction in the third layer of sand, respectively.

The bearing capacity on the caisson tip during installation with hardening in the third layer of sand, which is expressed as $\sigma_{zuH3}$, may be assumed utilizing the friction reduction factor $Fh_3$ given by Eq. (34) as follows

$$\sigma_{zuHk} = f_{BHk}\sigma_{zu} \qquad (k = 3) \tag{36}$$

$$f_{BHk} = exp(Fh_k - 1) \qquad (k = 3) \tag{37}$$

where $f_{BH3}$ is the bearing capacity reduction factor on the caisson tip in the third layer of sand.

### 5.5 The second silt hardening

Using Eq. (17), the value of $K_S\tan\delta$ at the caisson tip in the fourth layer of silt during installation with hardening subsequent to installation with hardening in the third layer of sand, which is written as $(K_S\tan\delta)_{H4}$, may be assumed in a simple form as follows

$$(K_S\,tan\delta)_{Hk} = Fh_k \cdot (K_S\,tan\delta)_{kN} \qquad (k = 4) \tag{38}$$

$$Fh_k = Kh_{Hk} \cdot Kh_{S(k-2)B} \cdot Kh_{H(k-2)P} \qquad (k = 4) \tag{39}$$

where the friction factor, $Kh_{H4}$, at the caisson tip in the fourth layer of silt during installation with hardening may be represented similarly to Eq. (25) for the first silt hardening as follows

$$Kh_{Hk} = \frac{s_{(k-1)L}}{s_k}\{1 - \beta(1 - \frac{h_{(k-1)L}}{h_k})\} \quad (k = 4) \tag{40}$$

where $s_4$ and $h_4$ are the suction and the penetration at the caisson tip in the fourth layer of silt, respectively. The bearing capacity on the caisson tip during installation with hardening in the fourth layer of silt, which is expressed as $\sigma_{zuH4}$, may be assumed utilizing the friction reduction factor $Fh_4$ given by Eq. (39) as follows

$$\sigma_{zuHk} = f_{BHk}\sigma_{zu} \quad (k = 4) \tag{41}$$

$$f_{BHk} = exp(Fh_k - 1) \quad (k = 4) \tag{42}$$

where $f_{BH4}$ is the bearing capacity reduction factor on the caisson tip in the fourth layer of silt.

The peak suction and the depth at the peak suction in the fourth layer of silt during installation with hardening are denoted by $s_{4P}$ and $h_{4P}$, respectively.

### 5.6 The second silt softening

The value of $K_S\tan\delta$ at the caisson tip during installation with softening in the fourth layer of silt subsequent to installation with hardening in the fourth layer of silt, which is represented as $(K_S\tan\delta)_{S4}$, may be assumed in a simple form as follows:

$$(K_S \, tan\delta)_{Sk} = Fh_k \cdot (K_S \, tan\delta)_{kN} \quad (k = 4) \tag{43}$$

$$Fh_k = Kh_{Sk} \cdot Kh_{HkP} \cdot Kh_{S(k-2)B} \cdot Kh_{H(k-2)P} \quad (k = 4) \tag{44}$$

where $Kh_{S4}$, which is the friction factor at the caisson tip in the fourth layer of silt during installation with softening, will be presented below, and $Kh_{H4P}$ is given by Eq. (40) with $s_4 = s_{4P}$ and $h_4 = h_{4P}$.

Similarly to Eq. (30) for the first silt softening, a simple form of $Kh_{S4}$ may be inferred as follows

$$Kh_{Sk} = 1 - \zeta(1 - \frac{h_{kP}}{h_k}\frac{s_k}{s_{kP}}) \quad (k = 4) \tag{45}$$

The bearing capacity on the caisson tip during installation with softening in the fourth layer of silt, which is written as $\sigma_{zuS4}$, may be assumed utilizing the friction reduction factor $Fh_4$ given by Eq. (44) in a simple form as follows

$$\sigma_{zuSk} = f_{BSk}\sigma_{zu} \quad (k = 4) \tag{46}$$

$$f_{BSk} = \frac{h_{kB} - h_k}{h_{kB} - h_{kP}} Fh_k \quad (k = 4) \tag{47}$$

where $f_{BS4}$ is the bearing capacity reduction factor on the caisson tip in the fourth layer of silt and $h_{4B}$ is the depth from the seabed to the bottom of the fourth layer of silt. The suction at the bottom of the fourth layer of silt is denoted by $s_{4B}$.

### 5.7 The third sand hardening

The value of $K_S\tan\delta$ at the caisson tip in the fifth layer of sand during installation with hardening subsequent to installation with softening in the fourth layer of silt, which is written as $(K_S\tan\delta)_{H5}$, may be assumed in a simple form as follows

$$(KS\tan\delta)Hk=Fhk\cdot(KS\tan\delta)kN\ (k=5) \tag{48}$$

$$Fh_k = Kh_{Hk} \cdot Kh_{S(k-1)B} \cdot Kh_{H(k-1)P} \cdot Kh_{S(k-3)B} \cdot Kh_{H(k-3)P} \quad (k = 5) \tag{49}$$

where $Kh_{S4B}$ is given by Eqs. (45) with $s_4 = s_{4B}$ and $h_4 = h_{4B}$, and similarly to Eq. (20) for the first sand hardening, $Kh_{H5}$ is represented by

$$Kh_{Hk} = \frac{s_{kL}}{s_k}\{1-\beta(1-\frac{h_{kL}}{h_k})\} \quad (k = 5) \tag{50}$$

where $s_{5L}$ and $h_{5L}$ are the suction and the depth at the onset of liquefaction in the fifth layer of sand, respectively, and $s_5$ and $h_5$ are the suction and the penetration at the caisson tip following liquefaction in the fifth layer of sand, respectively.

The bearing capacity on the caisson tip during installation with hardening in the fifth layer of sand, which is expressed as $\sigma_{zuH5}$, may be assumed utilizing the friction reduction factor $Fh_5$ given by Eq. (49) as follows

$$\sigma_{zuHk} = f_{BHk}\sigma_{zu} \quad (k = 5) \tag{51}$$

$$f_{BHk} = exp(Fh_k - 1) \quad (k = 5) \tag{52}$$

where $f_{BH5}$ is the bearing capacity reduction factor on the caisson tip in the fifth layer of sand.

For further installation of a suction caisson into the $k$-th soil layer $(6 \le k)$ in multilayered sand and silt, similarly to Eqs. (24), (29), (34), (39), (44), and (49), the friction reduction factor, $Fh_k$, on the caisson tip in the $k$-th soil layer can be determined combining by multiplication of the friction factors, $Kh_{Hj}$ and $Kh_{Sj}$ $(j \le k)$.

Consequently, new findings can be described as follows: For installation of suction caissons in multilayered sand and silt, the value of $(K_S\tan\delta)_i$ obtained from Eq. (17) in the $i$-th soil layer which is shallower than the $k$-th soil layer is attributed to the friction reduction factor, $Fh_k$, at the depth $h$ of the caisson tip in the $k$-th soil layer, which is given by Eqs. (24), (29), (34), (39), (44), and (49) in the case of three sand and two silt layers, for example.

## 6. Punching shear failure

Shallow foundations resting on a sand layer overlying a clay layer can sometimes break through the sand layer into the clay layer; e.g., Hanna and Meyerhof [24] and Okamura et al. [25]. This is known as punching shear failure. Similarly to the shallow foundations mentioned above, the experimental results obtained by Tran [15] and Tran et al. [16] indicated that a suction caisson that penetrates into the silt layer overlying a sand layer can break through the silt layer into the sand layer; i.e., punching shear failure can occur.

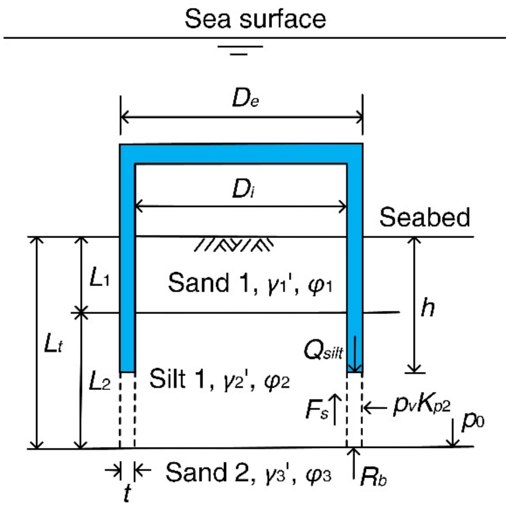


Figure 5. Relevant forces acting on the silt block assumed below the tip of suction caisson when punching shear failure occurs

Fig. 5 shows relevant forces acting on the silt block assumed below the tip of a suction caisson when punching shear failure occurs. According to the method proposed by Okamura et al. [25], equilibrium of the forces exerted on the silt block leads to the following

$$Q_{silt} = 2F_s + R_b - (L_t - h)\gamma_2' t \tag{53}$$

where $Q_{silt}$ is the ultimate vertical capacity on the silt block per unit length along the circumference and

$$F_s = (L_t - h)p_v K_{p2} tan\varphi_2 \tag{54}$$

$$p_v = \gamma_1' L_1 + \gamma_2'\{0.5(L_t + h) - L_1\} \tag{55}$$

$$R_b = q_{f3} t \tag{56}$$

$$q_{f3} = 0.5\gamma_3' t N_{\gamma 3} + p_0 N_{q3} \tag{57}$$

$$p_0 = \gamma_1' L_1 + \gamma_2' L_2 \tag{58}$$

where $L_1$ and $L_2$ are the thicknesses of sand 1 and silt 1, respectively, and $L_t = L_1 + L_2$; $K_{p2}$ is the coefficient of the Rankine passive pressure defined as $(1+\sin\varphi_2)/(1-\sin\varphi_2)$; $\varphi_1$, $\varphi_2$, and $\varphi_3$ are the angles of internal friction of sand 1, silt 1, and sand 2, respectively; $\gamma_1'$, $\gamma_2'$, and $\gamma_3'$ are the effective unit weights of sand 1, silt 1, and sand 2, respectively; $N_{\gamma 3}$ is the bearing capacity factor of sand 2 given by Michalowski [27]; and $N_{q3}$ is the bearing capacity factor of sand 2 presented by Reissner [28]. Eventually, the ultimate vertical capacity on the silt block in the silt layer overlying a sand bed under punching shear failure, $Q_b$, is represented as follows

$$Q_b = Q_{silt}\pi(D_i + D_e)/2 \tag{59}$$

The bearing capacity of the suction caisson in the silt layer, $Q_{tip}$ given by Eq. (14) satisfies Eq. (13) which represents the equilibrium of forces exerted on a suction caisson. Furthermore, equating Eq. (14) to Eq. (59), the penetration $h$ and the suction $s$ can be determined when punching shear failure occurs.

## 7. Numerical results

In many previous studies, laboratory and field tests have been carried out by assuming homogeneous soils in an attempt to mitigate problems related to the installation of suction caissons in real complex soil profiles. In contrast, there have been few experimental studies relevant to the installation of suction caissons in nonhomogeneous and layered soils. The validity of the procedure described in the present paper will be demonstrated by employing a limited number of tests from the literature to investigate the installation of suction caissons in sand and silt layers. Several illustrative examples are considered, and a comparison is made between the results from previous tests and those from the proposed method, as shown below. Most of the material constants presented in Tables 1-3 shown below were selected by calibrating the constants to match the simulated results with the experimental results.

### 7.1 Homogeneous sand

Kasuya et al. [30] examined the characteristics of the suction caisson installation in sand utilizing field tests. The installation tests included two suction caissons (named Caissons 1 and 2) in a medium dense sand; the dimensions of caissons and the properties of sands used in the tests are shown in Table 1. The buoyant unit weight of the caissons is $\gamma_c{}'$ = 68 kN/m$^3$. The submerged unit weight of the soil is denoted by $\gamma_{sub}{}'$. The parameter $(K_S\tan\delta)_{iN}$ shown in Eq. (17), which depends on the angle of internal friction of soil, is obtained from the values given by Poulos and Davis [31]. Through calibration using simulation and test data, the modification factor $m$ is assumed to be $m$ = 1.46. The installation was conducted with a penetration rate of 1.5 mm/s.

Fig. 6 shows the penetration produced by the penetration load during the installation of Caissons 1 and 2. The penetration load $P_L$ was defined as the sum of the buoyant weight of the caisson and the suction load applied below the internal lid area. It is predicted for Caisson 1 that during self-weight installation, the caisson reaches a penetration load ($P_L$) of 37.3 kN and penetration ($h$) of 0.53 m; suction installation is initiated and liquefaction occurs at $P_L$ = 81.0 kN and $h$ = 1.75 m. The predicted penetration increases linearly with penetration load, while the slope of the predicted curve during postliquefaction is slightly less than that during preliquefaction. It is predicted for Caisson 2 that the caisson settles down during self-weight installation at $P_L$ = 33.1 kN and $h$ = 0.43 m; liquefaction occurs at $P_L$ = 115 kN and $h$ = 1.92 m during suction installation. Good agreement is found between the observed and calculated values.

Houlsby and Byrne [11] presented a design procedure for installation of suction caissons in homogeneous sands and comparison was made with case records shown in Figs. 7-10 reported so far. In the current study, to simulate the above reported results, the caisson dimensions and sand properties in field tests are provided in Table 1. The value of $(K_S\tan\delta)_{iN}$ is deduced from the relationships between $(K_S\tan\delta)_{iN}$ and the angle of internal friction adduced by Poulos and Davis [31]. Calibrating the parameters used to match the simulated results with the experimental results,

Table 1. Caisson dimensions and sand properties in field tests

| Test name | $D_i$ | $h_c$ | $t$ | Caisson mass $M_c$ | Acceleration | $\varphi$ | $\gamma_{sub}'$ | $(K_S \tan\delta)_{iN}$ | $\beta$ | $k_f$ |
|---|---|---|---|---|---|---|---|---|---|---|
| | (m) | (m) | (mm) | (Mgrams) | (g-level) | ( ° ) | (kN/m$^3$) | | | |
| Caisson 1 | 1.8 | 4.6 | 19 | 3.72 | 1 | 36.6 | 9.0 | 0.5 | 0.0 | 1.0 |
| Caisson 2 | 2.3 | 3.0 | 19 | 3.38 | 1 | 36.6 | 9.0 | 0.5 | 0.0 | 1.0 |
| Tenby | 2.0 | 2.0 | 8 | 1.02 | 1 | 40.0 | 8.5 | 1.0 | 0.0 | 2.0 |
| Sandy Haven | 4.0 | 2.5 | 20 | 10.2 | 1 | 40.0 | 8.5 | 1.0 | 0.0 | 1.0 |
| Draupner E | 12.0 | 6.0 | 45 | 676 | 1 | 44.0 | 8.5 | 1.4 | 0.0 | 3.0 |
| Sleipner T | 15.0 | 5.0 | 45 | 1224 | 1 | 45.0 | 8.5 | 1.5 | 0.0 | 3.0 |

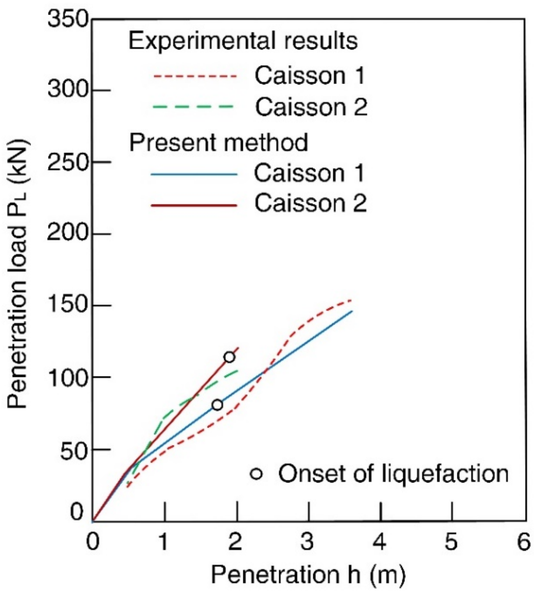


Figure 6. Penetration produced by penetration load during installation of Caissons 1 and 2

the modification factor $m$ is taken to be $m$ = 1.46, and the values of the initial ratio of the permeability $k_f$ are presented in Table 1.

Fig. 7 shows the penetration produced by suction during installation for the test name of *Tenby* presented by Houlsby and Byrne [11] in Table 1. It is predicted that the caisson reaches $h$ = 0.22 m during self-weight installation, suction installation commences, and liquefaction occurs at $s$ = 11.2 kPa and $h$ = 0.80 m.

Fig. 8 shows the penetration produced by suction regarding the test named *Sandy Haven* presented by Houlsby and Byrne [11] in Table 1. The prediction indicates that the caisson settles down during self-weight installation at $h$ = 0.44 m, suction installation starts, and liquefaction occurs at $s$ = 19.0 kPa and $h$ = 1.70 m.

Fig. 9 shows the penetration produced by suction for *Draupner E* described by Tjelta et al. [32, 33] in Table 1. It is predicted that the caisson arrives at $h$ = 1.80 m during self-weight installation, and liquefaction occurs at $s$ = 74.1 kPa and $h$ = 4.20 m during suction installation.

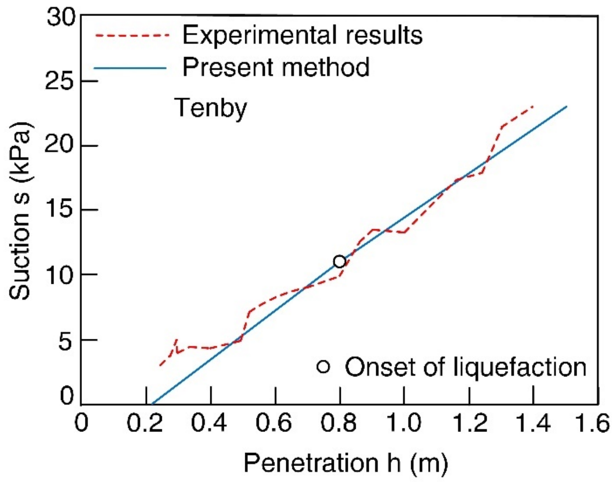


Figure 7. Penetration produced by suction during installation of Tenby

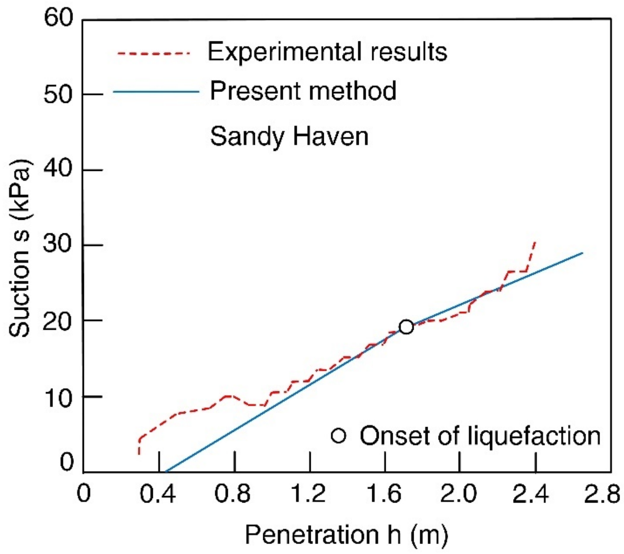


Figure 8. Penetration produced by suction during installation of Sandy Haven

Fig. 10 shows the penetration produced by suction about the test name of *Sleipner T* reported by Bye et al. [34] and Lacasse [35] in Table 1. The prediction indicates that the caisson settles down during self-weight installation at $h$ = 2.15 m; and liquefaction occurs at $s$ = 88.3 kPa and $h$ = 4.88 m during suction installation.

Figs. 7-10 reveal that the predicted penetration increases linearly with suction and that the slope of the predicted curve during postliquefaction is less than that during preliquefaction. Good agreement is found between the measured and predicted values.

Tran [15] and Tran et al. [16] carried out installation tests using a geotechnical centrifuge for suction caissons in sand and silt layers. Two types of soil, namely, silica sand and silt, were

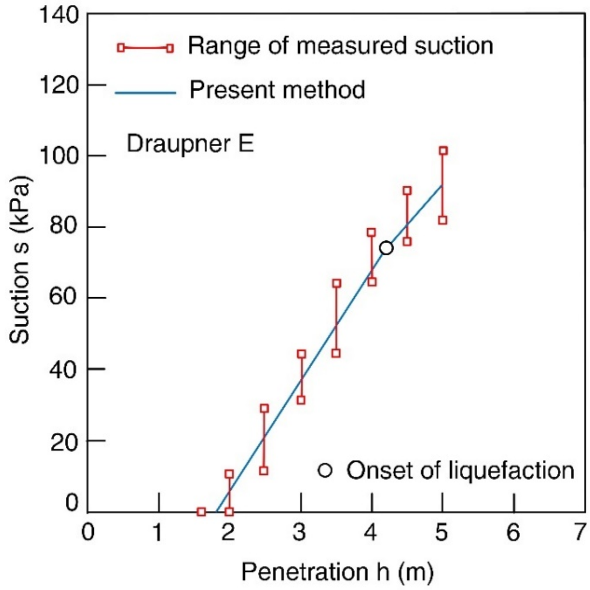


Figure 9. Penetration produced by suction during installation of Draupner E

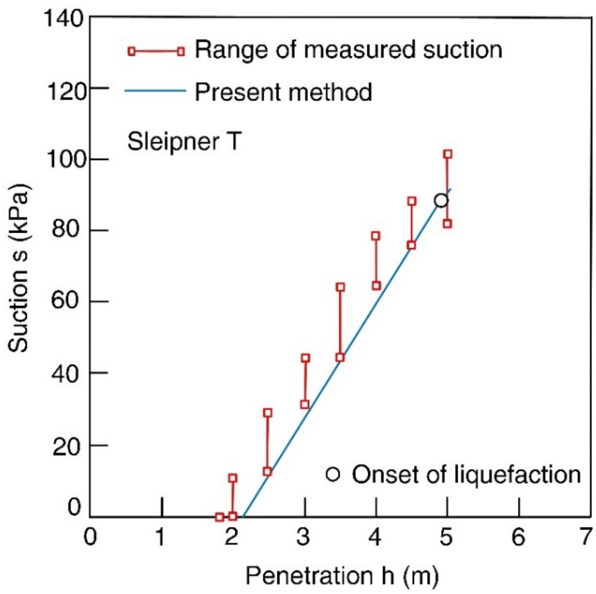


Figure 10. Penetration produced by suction during installation of Sleipner T

assumed to be nonplastic and noncohesive. In particular, the angle of internal friction of the silt employed in these tests was often higher than that of the sand. Since cone penetration tests (CPTs) for different soil profiles in tests were conducted, the angle of internal friction and $(K_S\tan\delta)_{iN}$ specified initially for sands and silts in each soil profile can be deduced by using the relevant correlations between CPT parameters presented by Schmertmann [36], Poulos and Davis [31],

Table 2. Caisson dimensions and sand properties in laboratory tests

| Test name | $D_i$ | $h_c$ | $t$ | Caisson mass $M_c$ | Accel-eration | $\varphi$ | $\gamma_{sub}'$ | $(K_S \tan\delta)_{iN}$ | $\beta$ | $k_f$ |
|---|---|---|---|---|---|---|---|---|---|---|
| | (mm) | (mm) | (mm) | (grams) | (g-level) | ( ° ) | (kN/m$^3$) | | | |
| S-60(0.5)-50 | 60 | 60 | 0.30 | 50 | 100 | 43 | 10 | 1.8 | 0.512 | 1.5 |
| S-60(0.5)-150 | 60 | 60 | 0.30 | 150 | 100 | 43 | 10 | 1.8 | 0.512 | 1.0 |
| S1g-100-260-S | 100 | 100 | 0.50 | 260 | 1 | 43 | 10 | 1.8 | 0.343 | 2.0 |
| S1g-100-260-F | 100 | 100 | 0.50 | 260 | 1 | 43 | 10 | 1.8 | 0.55 | 6.0 |
| S1g-70-260-S | 70 | 140 | 0.35 | 260 | 1 | 43 | 10 | 1.8 | 0.46 | 2.0 |
| S1g-70-260-F | 70 | 140 | 0.35 | 260 | 1 | 43 | 10 | 1.8 | 0.685 | 12.0 |

Robertson and Campanella [37], Kulhawy and Mayne [38], Jamiolkowski et al. [39], and Mayne [40]. The experimental results provided by Tran [15] and Tran et al. [16] are adopted in the caisson installation analysis shown below.

The caisson dimensions and properties of the homogeneous sand in the installation tests described by Tran [15] and Tran et al. [16] are specified in Table 2. The tests named S-60(0.5)-50 and S-60(0.5)-150 belong to the installation tests with an acceleration of 100 g, where the installation was conducted with a penetration rate (PR) of 0.1 mm/s. The following tests, namely, S1g-100-260-S with PR = 0.3 mm/s, S1g-100-260-F with PR = 6.5 mm/s, S1g-70-260-S with PR = 0.5 mm/s, and S1g-70-260-F with PR = 11 mm/s, are among the 1 g installation tests, where the end letters of S and F in the test names indicate slow and fast installations, respectively. The permeabilities of the silica sand and silt are approximately $1.0\times10^{-4}$ m/s and $1.3\times10^{-6}$ m/s, respectively. The experimental results given by Tran [15] indicate that the initial ratios of the permeability $k_f$ of S1g-100-260-F and S1g-70-260-F are 5.3 and 10.6, respectively; thus, the high values of $k_f$ = 6.0 and 12.0 are adopted for S1g-100-260-F and S1g-70-260-F in the present simulation, respectively. The modification factor $m$ is assumed to be $m$ = 1.46 through calibration between the simulation and experimental results, and this value is adopted in the following prediction.

Fig. 11 shows the penetration and hydraulic gradient along the inner caisson wall produced by suction for the S-60(0.5)-50 and S-60(0.5)-150 tests in Table 2. For the prediction of S-60(0.5)-50, the caisson reaches a normalized penetration (NP) of 0.084 during self-weight installation. The suction installation is started, and liquefaction occurs at the point of a normalized suction (NS) of 0.4 and NP = 0.25. The test results show that the hydraulic gradient $i$ during suction installation is developed as follows: first, a rapid increase in $i$ occurs up to the onset of liquefaction given by $i$ = 0.97, and then a relatively stable $i$ ensues during the remaining installation. Furthermore, for the prediction of S-60(0.5)-150, the caisson reaches NP = 0.161 during self-weight installation. Liquefaction occurs at NS = 0.45 and NP = 0.34 during suction installation. The predicted penetration increases linearly with suction, and the slope of the predicted curve during postliquefaction is distinct from that during preliquefaction. Good agreement is found between the measured and calculated values.

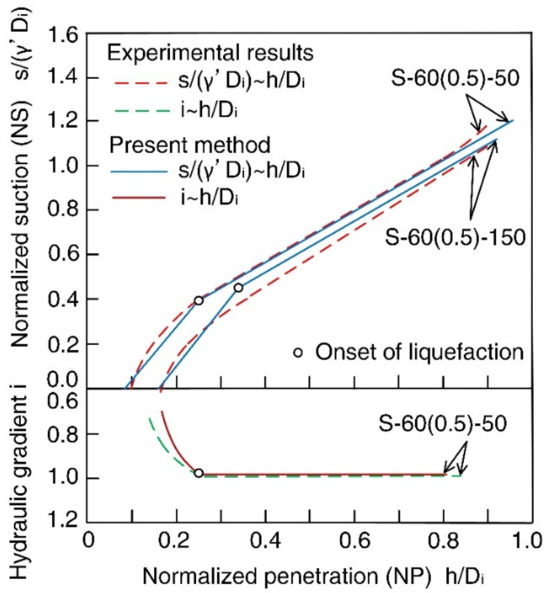


Figure 11. Penetration and hydraulic gradient along the inner caisson wall produced by suction

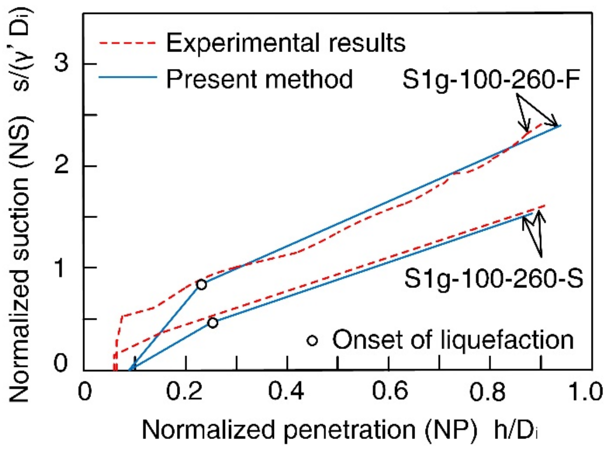


Figure 12. Penetration produced by suction during slow and fast installations when skirt length to diameter ratio is one

Fig. 12 shows the penetration produced by suction for the S1g-100-260-S and S1g-100-260-F tests in Table 2. For S1g-100-260-S, the caisson settles down during self-weight installation at NP = 0.09. The suction installation is slow, and liquefaction occurs at NS = 0.46 and NP = 0.25. For S1g-100-260-F, the caisson reaches NP = 0.09 during self-weight installation. The suction installation is fast, and liquefaction occurs at NS = 0.83 and NP = 0.23. The penetration predicted for the above two tests increases linearly with suction, and the slope of the predicted curve for postliquefaction is distinct from that for preliquefaction. For the effect of the installation rate on the suction in homogeneous sand, the faster the installation rate is, the greater the suction at the

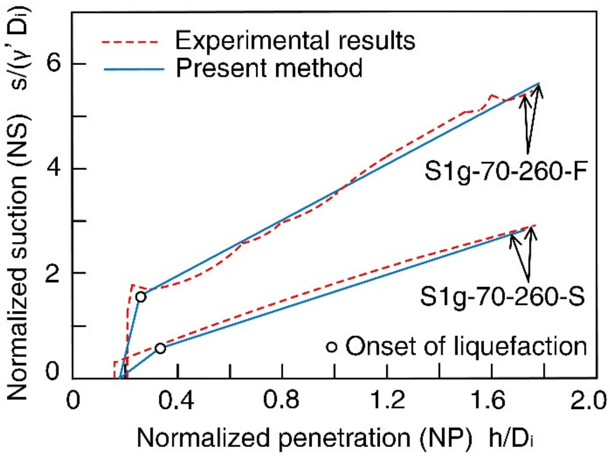


Figure 13. Penetration produced by suction during slow and fast installations when skirt length to diameter ratio is two

onset of liquefaction. Although the present method cannot capture some of the detail at the beginning of suction loading, the broad trend of the installation tests is predicted overall.

Fig. 13 shows the penetration produced by suction for the S1g-70-260-S and S1g-70-260-F tests in Table 2. For S1g-70-260-S, the caisson reaches NP =0.169 during self-weight installation. The suction installation starts slow, and liquefaction occurs at NS = 0.56 and NP = 0.33. For S1g-70-260-F, the caisson settles down during self-weight installation at NP = 0.169. The suction installation starts fast, and liquefaction occurs at NS = 1.52 and NP = 0.254. A comparison between the measured and predicted values of installation shows good agreement.

### 7.2 Sand and silt layers

Tran [15] and Tran et al. [16] conducted many installation tests, such as normal gravity (1 g) and centrifuge tests with an acceleration of 100 g for suction caissons in soil profiles where sand is overlain by a surficial layer of silt and sites where sand is interlayered by one or more bands of silt. The caisson dimensions and sand and silt properties used in installation tests named by Tran [15] and Tran et al. [16] are presented in Table 3. The angle of the internal friction of soil, $\varphi$, is deduced from the relationship among the cone tip resistance, depth, and relative density in experimental results, as mentioned above. The installation was carried out with PR= 0.1 mm/s. Tran [15] and Tran et al. [16] revealed that the scouring of silt along the inner wall in silt overlying sand induces the occurrence of the upward seepage flow in the silt layer. This suggests that the suction installation penetrating through the silt layer into a sand layer allows an upward seepage gradient to develop in the silt layer overlying the sand layer.

Fig. 14 shows the penetration produced by suction for the 1 m top silt-50 and 1 m top silt-150 tests in Table 3, where sand is overlain by a surficial layer of silt. For 1 m top silt-50, the caisson penetrates up to NP = 0.128 during self-weight installation. The suction installation starts with hardening in the silt layer, and the caisson tip arrives at the point of NS = 0.157 and NP =0.167 on the silt-sand interface. With increasing suction, liquefaction occurs at NS = 0.37 and NP = 0.27. For 1 m top silt-150, the caisson during self-weight installation reaches NP = 0.19, which is in the

Table 3. Caisson dimensions and sand-silt properties in centrifuge tests

| Test name | | 1 m top silt-50 | 1 m top silt-150 | 0.8 m deep silt-50 | 0.8 m deep silt-150 | 2 m deep silt-150 | 2 silt layers-50 |
|---|---|---|---|---|---|---|---|
| Caisson | $D_i$ (mm) | 60 | 60 | 60 | 60 | 60 | 60 |
| | $h_c$ (mm) | 60 | 60 | 60 | 60 | 60 | 60 |
| | $t$ (mm) | 0.3 | 0.3 | 0.3 | 0.3 | 0.3 | 0.3 |
| | Mass $M_c$ (grams) | 50 | 150 | 50 | 150 | 150 | 50 |
| Acceleration | g-level | 100 | 100 | 100 | 100 | 100 | 100 |
| Sand 1 | $\varphi$ ( ° ) | – | – | 43 | 43 | 38 | 41 |
| | $\gamma_{sub}'$ (kN/m$^3$) | – | – | 10 | 10 | 10 | 10 |
| | $(K_S \tan\delta)_{iN}$ | – | – | 1.8 | 1.8 | 1.0 | 1.0 |
| | $\beta$ | – | – | – | – | – | – |
| | $k_f$ | – | – | 1.5 | 1.5 | 1.5 | 1.5 |
| Silt 1 | $\varphi$ ( ° ) | 40 | 40 | 49 | 49 | 40 | 49 |
| | $\gamma_{sub}'$ (kN/m$^3$) | 10 | 10 | 10 | 10 | 10 | 10 |
| | $(K_S \tan\delta)_{iN}$ | 1.0 | 1.0 | 1.8 | 1.8 | 1.0 | 1.8 |
| | $\zeta$ | – | – | 0.288 | 0.024 | 0.062 | 0.0 |
| Sand 2 | $\varphi$ ( ° ) | 43 | 43 | 43 | 43 | 42 | 43 |
| | $\gamma_{sub}'$ (kN/m$^3$) | 10 | 10 | 10 | 10 | 10 | 10 |
| | $(K_S \tan\delta)_{iN}$ | 1.8 | 1.8 | 1.8 | 1.8 | 1.0 | 1.8 |
| | $\beta$ | 0.0 | 0.0 | 0.0 | 0.0 | 0.0 | 0.26 |
| | $k_f$ | 1.0 | 1.0 | variable | variable | variable | variable |
| Silt 2 | $\varphi$ ( ° ) | – | – | – | – | – | 49 |
| | $\gamma_{sub}'$ (kN/m$^3$) | – | – | – | – | – | 10 |
| | $(K_S \tan\delta)_{iN}$ | – | – | – | – | – | 1.8 |
| | $\zeta$ | – | – | – | – | – | −1.71 |
| Sand 3 | $\varphi$ ( ° ) | – | – | – | – | – | 43 |
| | $\gamma_{sub}'$ (kN/m$^3$) | – | – | – | – | – | 10 |
| | $(K_S \tan\delta)_{iN}$ | – | – | – | – | – | 1.8 |
| | $\beta$ | – | – | – | – | – | 0.26 |
| | $k_f$ | – | – | – | – | – | variable |

sand layer. Suction installation begins, and liquefaction occurs at NS = 0.45 and NP = 0.34. For the above two tests, the predicted penetration increases linearly with suction, and the slope of the predicted curve during postliquefaction is different from that during preliquefaction, except that the simulated curve of the installation during preliquefaction in the 1 m top silt-50 test shows nonlinearity. For the 1 m top silt-50 test, the experimental result was indicative of the occurrence of punching shear failure during the initial suction installation. However, the predicted results could not describe the feature of the punching shear failure. Although the present method cannot capture some of the details of suction installation, the broad trends of the tests can be predicted overall.

Fig. 15 shows the penetration produced by suction regarding the tests of 0.8 m deep silt-50 and 0.8 m deep silt-150 in Table 3, where the silt layer below a thin upper sand surface is overlying a lower sand layer. For the prediction of 0.8 m deep silt-50, the caisson penetrates up to NP = 0.084 during self-weight installation. The suction installation is started, and the tip arrives at the point of NS = 0.12 and NP = 0.133 on the sand-silt interface. With penetration of the tip into the silt layer

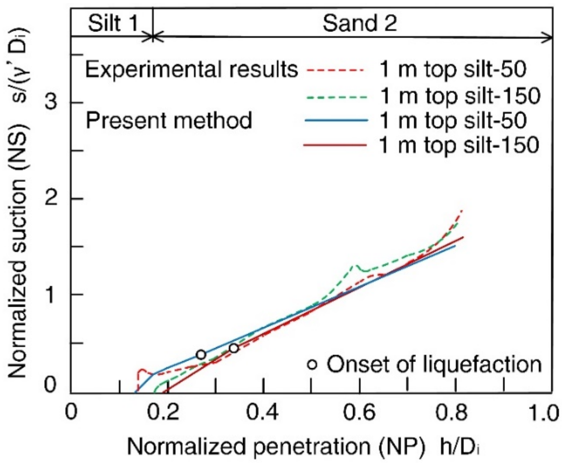


Figure 14. Penetration produced by suction when sand layer is overlain by surficial layer of silt

due to the suction installation, hardening develops in the silt layer, and the tip arrives at the peak point of NS = 2.47 and NP = 0.2, where punching shear failure arises. After reaching the peak of suction, softening occurs, and the tip arrives at a point on the silt-lower sand interface, which is given by NS = 0.6 and NP = 0.3. During the installation that keeps the caisson tip in the silt layer, no seepage flow can be assumed because of the low permeability of the silt layer. At the instant that the skirt tip penetrates through the silt layer into the lower sand layer, seepage flow and liquefaction occur because of the scouring of the silt layer. Then the suction increases again with further penetration. For the prediction of 0.8 m deep silt-150 in Fig. 15, the caisson tip reaches the sand-silt interface at NP = 0.133 during self-weight installation. Then, suction installation is commenced. As the installation proceeds, hardening develops in the silt layer, and the tip arrives at the peak point of NS = 1.87 and NP = 0.2, where punching shear failure occurs. Following the peak of suction, softening ensues, and the skirt tip reaches the point of NS = 0.521 and NP = 0.3 at the silt-lower sand interface. The instant that the caisson tip penetrates through the silt layer into the lower sand layer, seepage flow and liquefaction occur. Finally, the suction increases with increased penetration.

Fig. 16 shows the penetration produced by suction regarding the test of 2 m deep silt-150 in Table 3, where the silt layer below a thick upper sand surface is overlying a lower sand layer. Taking into account the lower relative density of 60% of the sand above the silt from experimental results, the angle of internal friction and $(K_S\tan\delta)_{iN}$ of soils were determined. The results indicate that the caisson settles down during self-weight installation at NP = 0.285 in the upper sand layer. The suction installation is started, and the tip arrives at the point of NS = 0.142 and NP = 0.333 at the sand-silt interface. When penetrating the tip into the silt layer, hardening develops in the silt layer and the tip arrives at the peak point of NS = 2.04 and NP = 0.46, where punching shear failure arises. After reaching the peak of suction, softening appears and the tip reaches a point at the silt-lower sand interface, which is given by NS =0.9 and NP = 0.5. During the suction installation in the silt layer, no seepage flow is assumed because of the low permeability of the silt layer. The instant that the skirt tip penetrates through the silt layer into the lower sand layer, seepage flow and liquefaction occur because of the scouring of the silt layer. Then the suction increases again with further penetration.

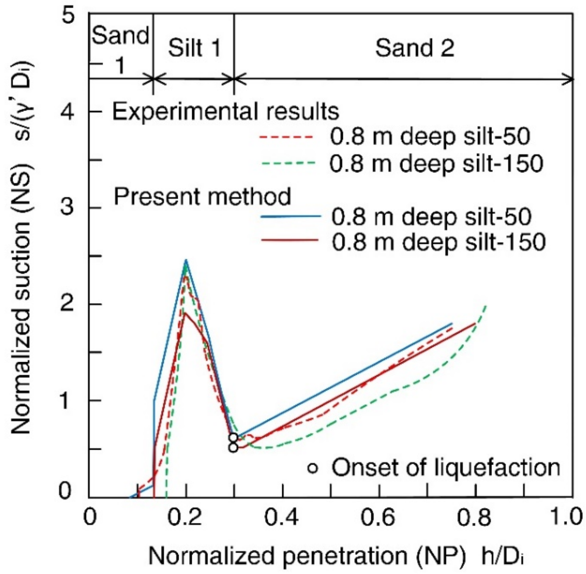


Figure 15. Penetration produced by suction when the silt layer below thin upper sand surface is overlying lower sand layer

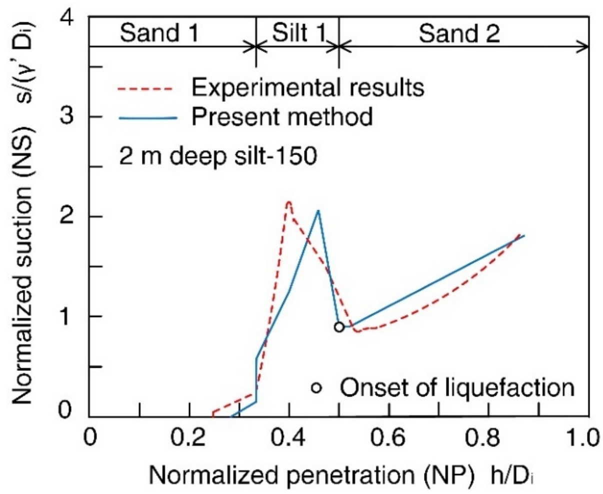


Figure 16. Penetration produced by suction when the silt layer below thick upper sand surface is overlying lower sand layer

Fig. 17 shows the penetration produced by suction regarding the 2 silt-layers-50 test in Table 3, where the soil profile consists of two silt layers and three sand layers. In this case, the caisson settles at NP = 0.13 during self-weight installation. The suction installation begins, and the tip arrives at the point of NS = 0.07 and NP = 0.167 at sand 1-silt 1 interface. With the penetration of the skirt tip into silt 1, hardening develops and the tip arrives at the peak point of NS = 1.38 and NP = 0.184 in silt 1, where punching shear failure occurs. After reaching the peak of suction, softening ensues and the tip reaches a top point of sand 2, which is given by NS = 0.4 and NP =

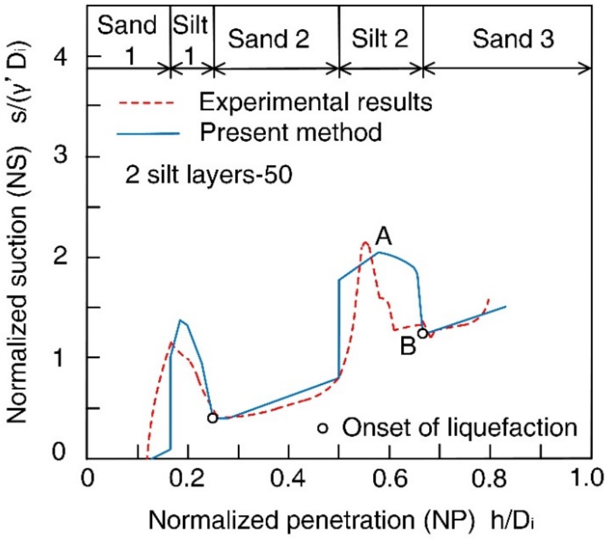


Figure 17. Penetration produced by suction during installation through two silt layers in three sand layers

0.25. The instant that the tip penetrates into sand 2, seepage flow and liquefaction occur because of the scouring of silt 1. Then, the suction increases again with further penetration, and the tip arrives at the point of NS = 0.8 and NP = 0.5 at sand 2-silt 2 interface. As the suction installation proceeds, hardening develops and the tip arrives at the peak point of NS = 2.05 and NP = 0.58 in silt 2, where punching shear failure occurs. Following the peak of suction, softening appears, and the skirt tip reaches the point of NS = 1.25 and NP = 0.667 at silt 2-sand 3 interface. Finally, the instant that the tip penetrates into sand 3, seepage flow and liquefaction occur because of the scouring of silt 2. Following this, the suction increases again with further penetration. During the installation with softening from point $A$ to $B$ in silt 2, the softening constant $\zeta$ takes a negative value which is different from the positive values deduced from the installation with softening in silt 1 in Fig. 17 and the silt layers in the other tests shown in Table 3. This is because since $(K_S\tan\delta)_{S4}$ of Eq. (43) in the fourth layer of silt during installation with softening needs to have a large value to satisfy the equilibrium provided by Eq. (13), the softening constant $\zeta$ in the friction factor of the fourth layer of silt given by $Kh_{S4}$ of Eq. (45) eventuates in the negative value.

Figs. 14-17 indicate that although the present method cannot capture some of the details during the installation of suction caissons in sand and silt layers, the broad trend of the centrifuge tests can be predicted overall.

In case that the present classical bearing-capacity formulation is extended to plastic/cohesive low-permeability layers, a further developed investigation is needed by overcoming the several limitations of nonplastic and noncohesive soils assumed in the current paper.

## 8. Conclusions

An analytical investigation was carried out using a classical bearing capacity approach to elucidate the characteristics of installation of suction caissons in multilayered sand and silt. The conclusions are summarized as follows:

- Considering the occurrence of sand liquefaction during suction installation of caissons, the relationships between the suction and the penetration were revealed analytically for both preliquefaction and postliquefaction.
- Taking into account the characteristics of the unit shaft and base resistances of suction caissons during installation, the friction reduction factor along the caisson skirt and the bearing capacity reduction factor on the caisson tip were proposed for installation with both hardening and softening in multilayered soils.
- For the punching shear failure induced by the installation of a suction caisson in the silt layer overlying a sand layer, an analytical procedure using the equilibrium of forces exerted on the silt block was presented.
- Regarding the relationships between the suction and penetration in multilayered sand and silt during installation, good agreement was found between the results obtained from field and centrifuge tests and those predicted by the present method.

## Acknowledgements

The research described in this paper was financially supported by Applied Geotechnical Institute, Inc. This corporation is engaged in the development of analytical methods for design of suction caisson anchors connected to floating offshore wind turbines via mooring systems. The author would like to express a feeling of gratitude for the outcome that the above support made it possible to achieve the comprehensive analytical approaches for installation of suction caissons in multilayered soils.

## References

1. Hirai, H. (2017). Evaluation of pullout load capacity of suction caissons in sand using a three-dimensional displacement approach. Marine Georesources & Geotechnology, 35(8), 1121-1134. https://doi.org/10.1080/1064119X.2017.12951207.
2. Hirai, H. (2018a). Analysis of laterally loaded bucket foundation with external skirt in sand using a Winkler model approach. Ocean Engineering, 147, 30-44. https://doi.org/10.1016/j.oceaneng.2017.10.007.
3. Hirai, H. (2018b). Analysis of pullout load capacity of suction caissons in clay by a three-dimensional displacement approach. Marine Georesources & Geotechnology, 36(4), 425-437. https://doi.org/10.1080/1064119X.2017.1326070.
4. Hirai, H. (2020). Analysis of cylindrical and rectangular bucket foundations subjected to vertical and lateral loads in sand using a three-dimensional displacement approach. Soils and Foundations, 60(1), 45-62. https://doi.org/10.1016/j.sandf.2020.01.001.
5. Hirai, H. (2022). Failure surface for shallow foundations in sand using a classical bearing capacity. Soils and Foundations, 62(2), 101125. https://doi.org/10.1016/j.sandf.2022.101125.
6. Hirai, H. (2023a). Failure envelope considering the ultimate tensile capacity of suction caissons in sand. Soils and Foundations, 63(3), 101311. https://doi.org/10.1016/j.sandf.2023.101311.
7. Hirai, H. (2023b). Failure surface considering the ultimate tensile and compressive capacities of suction caissons in clay. Marine Georesources & Geotechnology, 41(8), 884-894. https://doi.org/10.1080/1064119X.2022.2107465.
8. Hirai, H. (2025). Analysis of suction caisson anchors in sand connected to floating offshore wind turbines via catenary mooring using a three-dimensional displacement method. International Journal of Geotechnical Engineering, 19(4), 172-184. https://doi.org/10.1080/19386362.2025.2459278.

9. Erbrich, C.T., Tjelta, T.I. (1999). Installation of bucket foundations and suction caissons in sand— Geotechnical performance. Proceedings of the Offshore Technology Conference, Houston, TX, USA.
10. Houlsby, G.T., Byrne, B.W. (2005a). Design procedures for installation of suction caissons in clay and other materials. Proceedings of the Institution of Civil Engineers-Geotechnical Engineering, 158(2), 75-82. https://doi.org/10.1680/geng.158.2.75.61630.
11. Houlsby, G.T., Byrne, B.W. (2005b). Design procedures for installation of suction caissons in sand Proceedings of the Institution of Civil Engineers-Geotechnical Engineering, 158(3), 135-144. https://doi.org/10.1680/geng.158.3.135.66297.
12. Senders, M., Randolph, M.F. (2009). CPT-based method for the installation of suction caissons in sand. Journal of Geotechnical and Geoenvironmental Engineering, 135(1), 14-25. https://doi.org/10.1061/(ASCE)1090-0241(2009)135:1(14).
13. Koteras, A.K., Ibsen, L.B. (2018). Medium-scale laboratory model of mono-bucket foundation for installation tests in sand. Canadian Geotechnical Journal, 56(8), 1142-1153. https://doi.org/10.1139/cgj-2018-0134.
14. Rodriguez, F.M.G., Ibsen, L.B., Koteras, A.K., Barari, A. (2022). Investigation of the penetration resistance coefficients for the CPT-based method for suction bucket foundation installation in sand. International Journal of Geomechanics, 22(6), 04022063. https://doi.org/10.1061/(ASCE)GM.1943-5622.0002370.
15. Tran, M.N. (2005). Installation of suction caissons in dense sand and the influence of silt and cemented layers. Ph.D. Dissertation, University of Sydney, Sydney, Australia.
16. Tran, M.N., Randolph, M.F., Airey, D.W. (2007). Installation of suction caissons in sand with silt layers. Journal of Geotechnical and Geoenvironmental Engineering, 133(10), 1183-1191. https://doi.org/10.1061/(ASCE)1090-0241(2007)133:10(1183).
17. Ragni, R., Bienen, B., O'Loughlin, C.D., Stanier, S.A., Cassidy, M.J., Morgan, N. (2020). Observations of the effects of a clay layer on suction bucket installation in sand. Journal of Geotechnical and Geoenvironmental Engineering, 146(5), 04020020. https://doi.org/10.1061/(ASCE)GT.1943-5606.0002217.
18. Stapelfeldt, M., Bienen, B., Grabe, J. (2021). Influence of low-permeability layers on the installation and the response to vertical cyclic loading of suction caissons. Journal of Geotechnical and Geoenvironmental Engineering, 147(8), 04021076. https://doi.org/10.1061/(ASCE)GT.1943-5606.0002522.
19. Kerisel, J.L. (1962). Foundations profondes en milieu sableux. Proceedings of the 5th ICSMFE, 2, 73-83.
20. Vesić, A.S. (1964). Ultimate loads and settlements of foundations in sand. Symp. Bearing Capacity and Settlement of Foundations, Duke University, 53-67.
21. BCP Committee (1971). Field tests on piles in sand. Soils and Foundations, 11(2), 29-49. https://doi.org/10.3208/sandf1960.11.2_29.
22. Hanna, T.H., Tan, R.H.S. (1973). The behavior of long piles under compressive loads in sands. Canadian Geotechnical Journal, 10(3), 311-340. https://doi.org/10.1139/t73-030.
23. Zhang, P., Ding, H., Le, C. (2013). Installation and removal records of field trials for two mooring dolphin platforms with three suction caissons. Journal of Waterway, Port, Coastal, and Ocean Engineering, 139(6), 502-517. https://doi.org/10.1061/(ASCE)WW.1943-5460.0000206.
24. Hanna, A., Meyerhof, G.G. (1980). Design charts for ultimate bearing capacity of foundations on sand overlying soft clay. Canadian Geotechnical Journal, 17, 300-303. https://doi.org/10.1139/t80-030.
25. Okamura, M., Takemura, J., Kimura, T. (1998). Bearing capacity predictions of sand overlying clay based on limit equilibrium methods. Soils and Foundations, 38(1), 181-194. https://doi.org/10.3208/sandf.38.181.
26. Janssen, H.A. (1895). Versuche über Getreidedruck inSilozellen. Verein Deutscher Ingenieure Zeitschrift, Düsseldorf, 39, 1045-1049.
27. Michalowski, R.L. (1997). An estimate of the influence of soil weight on bearing capacity using limit analysis. Soils and Foundations, 37(4), 57-64. https://doi.org/10.3208/sandf.37.4_57.

28. Reissner, H. (1924). Zum Erddruckproblem. Proceedings of the 1st Int. Congress for Applied Mechanics, Biezeno CB and Burgers JM (eds), Delft, The Netherland.
29. Pande, G.N., Zienkiewicz, O.C. (1982). Soil mechanics – transient and cyclic loads. John Wiley & Sons, New York, NY, USA.
30. Kasuya, Y., Ito, M., Hayashi, H., Yamada, Y., Takahashi, S. (2016). Study on pullout resistance of skirt suction anchor for floating offshore windmill. Report of the Engineering Research Laboratory, Ohbayashi-Gumi Ltd, Japan, 80, 1-10.
31. Poulos, H.G., Davis, E.H. (1980). Pile foundation analysis and design. John Wiley & Sons, New York, NY, USA.
32. Tjelta, T.I. (1994). Geotechnical aspects of bucket foundations replacing piles for the Europipe 16/11-E. Proceedings of the Offshore Technology Conference, Houston TX, USA.
33. Tjelta, T.I. (1995). Geotechnical experience from the installation of the Europipe Jacket with bucket foundations. Proceedings of the Offshore Technology Conference, Houston, TX, USA.
34. Bye, A., Erbrich, C.T., Rognlien, B., Tjelta, T.L. (1995). Geotechnical design of bucket foundations. Proceedings of the Offshore Technology Conference, Houston, TX, USA.
35. Lacasse, S. (1999). Ninth OTRC Honors Lecture: Geotechnical contributions to offshore development. Proceedings of the Offshore Technology Conference, Houston TX, USA. https://doi.org/10.4043/10822-MS.
36. Schmertmann, J.H. (1978). Guidelines for cone penetration tests, performance and design, Report FHWA-TS-78-209, Federal Highway Administration, Washington, DC, USA.
37. Robertson, P.K., Campanella, R.G. (1983). Interpretation of cone penetration tests ─ Part I (Sand). Canadian Geotechnical Journal, 20(4), 718-733. https://doi.org/10.1139/t83-078.
38. Kulhawy, F.H., Mayne, P.W. (1990). Manual on estimating soil properties for foundation design. Report EL-6800, Electric Power Research Institute.
39. Jamiolkowski, M., LoPresti, D.C.F., Manassero, M. (2001). Evaluation of relative density and shear strength of sands from cone penetration test and flat dilatometer test, ASCE Geotechnical Special Publication, No. 119, 201-238.
40. Mayne, P.W. (2014). Interpretation of geotechnical parameters from seismic piezocone tests. Proceedings 3rd Int Symp on Cone Penetration Testing (CPT'14 Las Vegas), ISSMGE Technical Committee TC 102, (Eds., Robertson, P.K., Cabal, K.I.), 47-73.

## Nomenclature

Romans

| | |
|---|---|
| $a$ | Pressure factor at tip of caisson, Eq. (16) |
| $a_1$ | Pressure factor by Houlsby and Byrne |
| $A_i$ | Area of internal soil disc |
| $D_e$ | External diameter |
| $D_i$ | Internal diameter |
| $f_{BHk}$ | Bearing capacity reduction factor on caisson tip in the $k$-th layer during hardening, Eq. (22) |
| $f_{BSk}$ | Bearing capacity reduction factor on caisson tip in the $k$-th layer during softening, Eq. (32) |
| $Fh_k$ | Friction reduction factor at caisson tip in the $k$-th soil layer, Eq. (17) |
| $h$ | Penetration depth from seabed to skirt tip |
| $h_c$ | Skirt length |
| $h_k$ | Penetration at caisson tip in the $k$-th layer |
| $h_{kB}$ | Depth from seabed to bottom of the $k$-th layer |
| $h_{kL}$ | Depth at onset of liquefaction in the $k$-th layer |
| $h_{kP}$ | Depth at peak suction in the $k$-th layer |
| $h_w$ | Water depth |
| $H_m$ | Thickness of the $m$-th layer |
| $k_e$ | Permeability of soil outside caisson |
| $k_i$ | Permeability of soil inside caisson |
| $k_f$ | Permeability ratio |
| $Kh_{Hk}$ | Friction factor at caisson tip in the $k$-th layer during hardening, Eq. (20) |
| $Kh_{Sk}$ | Friction factor at caisson tip in the $k$-th layer during softening, Eq. (30) |
| $K_p$ | Coefficient of Rankine passive pressure |
| $K_S$ | Coefficient of lateral pressure |
| $(K_S\tan\delta)_k$ | Value for the $k$-th soil layer during installation, Eq. (17) |
| $(K_S\tan\delta)_{kN}$ | Value for the $k$-th soil layer specified initially, Eq. (17) |
| $L_k$ | Thickness of the $k$-th layer |
| $m$ | Modification factor |
| $mb$ | Soil layer under tip of caisson |
| $n$ | Number of layers of nonhomogeneous soil |
| $N_q$ | Bearing capacity factor by Reissner |
| $N_{qk}$ | Bearing capacity factor of the $k$-th layer by Reissner |
| $N_\gamma$ | Bearing capacity factor by Michalowski, Eq. (12) |
| $N_{\gamma k}$ | Bearing capacity factor of the $k$-th layer by Michalowski |
| $p_a$ | Atmospheric pressure |
| $P_{em}$ | External vertical traction along the $m$-th element |
| $P_{im}$ | Internal vertical traction along the $m$-th element |
| $P_L$ | Penetration load |
| $P_{Vm}$ | Vertical force along the $m$-th element |
| $P_{Vye}$ | Vertical yield resistance of soil outside skirt, Eq. (8) |
| $P_{Vyi}$ | Vertical yield resistance of soil inside skirt, Eq. (9) |
| $Q_b$ | Ultimate vertical capacity on silt block, Eq. (59) |
| $Q_{silt}$ | Ultimate vertical capacity on silt block per unit length, Eq. (53) |
| $Q_{tip}$ | Bearing capacity on annulus of caisson tip, Eq. (14) |
| $s$ | Excess pore pressure (suction), Eq. (15) |
| $s_k$ | Suction at caisson tip in the $k$-th layer |
| $s_{kB}$ | Bottom suction in the $k$-th layer |

| | |
|---|---|
| $s_{kL}$ | Suction at onset of liquefaction in the *k*-th layer |
| $s_{kP}$ | Peak suction in the *k*-th layer |
| $t$ | Thickness of the lid or skirt |
| $V$ | Vertical compressive load |
| $V_{mb}$ | Vertical force on the *mb*-th layer |
| $W_c$ | Buoyant weight of suction caisson |
| $(x, y, z)$ | Rectangular Cartesian coordinate system |

Greeks

| | |
|---|---|
| $\beta$ | Hardening constant, Eq. (20) |
| $\gamma'$ | Effective unit weight of soil |
| $\gamma_c'$ | Buoyant unit weight of caisson |
| $\gamma_e'$ | Effective unit weight of external soil |
| $\gamma_i'$ | Effective unit weight of internal soil |
| $\gamma'_{ij}, \gamma'_{ej}, \mu_{ij}, \mu_{ej}$ | $\gamma'_i, \gamma'_e, \mu_i, \mu_e$ of the *j*th layer |
| $\gamma_{sub}'$ | Submerged unit weight of soil |
| $\gamma_w$ | Unit weight of water |
| $\delta$ | Interface friction angle between soil and skirt |
| $\zeta$ | Softening constant, Eq. (30) |
| $\mu_e$ | Vertical pressure factor outside skirt, Eq. (6) |
| $\mu_i$ | Vertical pressure factor inside skirt, Eq. (2) |
| $\sigma'_{be}$ | Effective vertical stresses in soil outside skirt tip, Eq. (10) |
| $\sigma'_{bi}$ | Effective vertical stresses in soil inside skirt tip, Eq. (11) |
| $\sigma'_{ze}$ | Effective vertical pressure outside skirt, Eq. (5) |
| $\sigma'_{zi}$ | Effective vertical pressure inside skirt, Eq. (4) |
| $\sigma_{zu}$ | Smaller of bearing capacities, Eq. (14) |
| $\sigma_{zue}$ | Ultimate base resistance (bearing capacity) outside skirt, Eq. (10) |
| $\sigma_{zuHk}$ | Bearing capacity on caisson tip during hardening in the *k*-th layer, Eq. (21) |
| $\sigma_{zui}$ | Ultimate base resistance (bearing capacity) inside skirt, Eq. (11) |
| $\sigma_{zuSk}$ | Bearing capacity on caisson tip during softening in the *k*-th layer, Eq. (31) |
| $\varphi$ | Angle of internal friction of soil |
| $\varphi_k$ | Internal friction angle of soil of the *k*-th layer |

Subscripts

| | |
|---|---|
| *b* | Block |
| *B* | Bearing capacity or Bottom |
| *e* | External |
| *H* | Hardening |
| *i* | Internal |
| *k* | *K*-th layer |
| *L* | Liquefaction |
| *N* | Natural |
| *P* | Peak |
| *S* | Softening |
| *u* | Ultimate |
| *z* | Vertical direction |

Acronyms

| | |
|---|---|
| NP | Normalized penetration |
| NS | Normalized suction |
| PR | Penetration rate |